AIChE

Scalar Mixing by Granular Particles

J. J. Derksen
Chemical and Materials Engineering Dept., University of Alberta, Edmonton, Alberta, T6G 2G6 Canada

DOI 10.1002/aic.11519
Published online May 13, 2008 in Wiley InterScience (www.interscience.wiley.com).

We study by direct numerical simulation the role of spherical, solid, uniformly sized, moving particles immersed in a fluid in spreading a passive scalar with high Schmidt number dissolved in the fluid. The solid particles are one-way coupled to the fluid: they agitate the fluid but they do not feel the presence of the fluid (they move as a granular gas). The two independent variables in the simulations are the solids volume fraction that we vary in the range of 10–45%, and the granular Reynolds number, based on the particle diameter and the granular temperature, which has been varied from 2.8 to 280. It is shown that the scalar spreading rate strongly decreases with increasing solids volume fraction; the spreading appears to scale quite well with the mean free path of the particles. At increasing granular Reynolds number the fluid flow develops more small scale structures that enhance scalar spreading. We propose a relation for an effective diffusion coefficient that describes the scalar spreading in terms of the independent variables. © 2008 American Institute of Chemical Engineers *AIChE J,* 54: 1741–1747, 2008
Keywords: computational fluid dynamics (CFD), multi-phase flow, mixing

Introduction

The simulation of dense gas-solid and liquid-solid flows has great relevance for many applications in chemical and environmental engineering. A large body of research has been devoted to capture the dynamics of such systems in sets of continuum equations, including closures,[1,2] and in devising efficient numerical schemes to solve these. In continuum approaches, the kinetics of individual particles is represented by their collective transport properties in a way akin to classical kinetic theory. Driven by on one side increased computer hardware performance, and progress in numerical methods, on the other side a desire to reveal the often rate limiting processes at the particle scale, discrete particle methods (DPM) are being developed. In the DPM the motion of each individual particle (including its collision with other particles and with walls) is tracked, whereas the interstitial gas or liquid flow is solved in an approximate manner.[3,4] Strong computers and fast algorithms nowadays allow for DPM simulations with many thousands of particles[5] thus allowing for realistic simulations of meso-scale effects in process equipment.

Correspondence concerning this article should be addressed to J. J. Derksen at jos@ualberta.ca.

In chemical engineering, the applications driving the above developments, however, usually involve more than the fluid and granular dynamics, heat and (reactive) mass transfer being prominent examples. To model the transport of a scalar in the continuous phase, somehow the role of the particles in the dispersion of the scalar needs to be taken into account. So far this modeling is largely based on empirical dispersion models as they can be found in e.g. the monograph by Levenspiel[6] and references therein. Interpretation of experimental results on e.g. gas mixing in fluidized beds[7–9] would benefit from a more fundamental understanding of the contribution of solids to scalar dispersion.

Also—in the context of computational fluid dynamics (CFD) of turbulent disperse multiphase flows—it is quite common to apply the analogy of transport of momentum by eddies and of a scalar for estimating scalar eddy diffusion/dispersion coefficients. It is questionable if such an approach would be valid for systems with high volumetric disperse phase loadings. In dense systems turbulence can hardly develop due to the small interparticle spacings, leaving an eddy diffusivity concept without a firm physical basis.

In the present study, numerical experiments are described that directly probe the spreading of a passive scalar as a result of solid particle motion. The moving particles agitate the interstitial fluid. Subsequently the flow disperses the

scalar dissolved in the fluid. Goals of the simulations are to find out how the scalar spreading scales with the parameters governing the particle and fluid motion such as the granular temperature, the mean free path of the particles and the fluid's viscosity, and to propose expressions for scalar dispersion coefficients.

The systems we study numerically consist of three-dimensional periodic domains that contain solid particles and interstitial fluid. The particles move as a granular gas with a constant temperature, i.e. they move ballisticly through the fluid and undergo fully elastic and smooth collisions. The particles do not feel the presence of the fluid. At the fluid-solid interfaces, however, we impose a no-slip condition on the fluid. In that manner the fluid responds to the particle motion and gets agitated. Once this fluid-solid system is fully developed we release a passive scalar in the fluid phase. By solving the convection equation for the tracer with nonpenetration boundary conditions at the solid surfaces, we observe how the tracer spreads by the action of the moving solid particles only. We do not consider mass transfer between the particles and the fluid, the solid particles are only there to agitate the fluid and thus mix the scalar dissolved in the fluid phase.

The primary independent variables in the numerical experiments are the solids phase volume fraction ϕ, and the Reynolds number based on the granular temperature T_g of the particles $Re_g = \sqrt{T_g}\, d_p/v$, with d_p the particle diameter, and v the fluid's kinematic viscosity. To limit the parameter space, we give the dissolved scalar a very high Schmidt number, i.e. we set the molecular diffusivity of the passive scalar to zero. The (inevitable) numerical diffusion is suppressed by using a total variation diminishing (TVD) scheme in estimating convective fluxes.[10] The level of numerical diffusion is assessed by checking the effect of grid refinement.

Numerical Procedure

We consider a fully periodic, three-dimensional, cubic domain with edge length L. In this cube we release N spherical particles all having the same diameter d_p. The solids volume fraction of the system is $\phi = N\frac{\pi d_p^3}{6L^3}$. The particles are given a mean-square velocity of $2T_g$, with T_g the granular temperature. The energy of the particulate system is fully contained in translational motion—the particles do not rotate. The granular temperature is kept constant by letting the particles undergo fully elastic and frictionless hard-sphere collisions. After this (dry) granular system has evolved to a steady state, we introduce the interstitial fluid. This fluid is one-way coupled to the particles: the fluid responds to the particle motion; the particles do not feel the fluid and continue their granular motion.

The fluid flow we solve with the lattice-Boltzmann method (LBM). For flows in complexly shaped domains with moving boundaries, this method has proven its usefulness (see e.g. the review article by Chen & Doolen[11]). In the LBM, the computational domain is discretized into a number of lattice nodes residing on a uniform, cubic grid. Fluid parcels move from each node to its neighbors according to prescribed rules. It can be proven by means of a Chapman-Enskog expansion that, with the proper grid topology and collision rules, this system obeys, in the low Mach number limit, the incompressible Navier-Stokes equations.[11,12] The specific implementation used in our simulations has been described by Somers,[13] which is a variant of the widely used Lattice BGK scheme to handle the collision integral (e.g., see Qian et al.[14]). We use the scheme due to Somers, as it manifests a more stable behaviour at low viscosities when compared to LBGK.

In our code, the no-slip condition at the solid-fluid boundaries is introduced through a forcing scheme.[15–17] The forcing scheme is akin to immersed boundary methods that have been developed by among others Peskin and coworkers.[18] The particle motion drives the fluid flow by demanding that at the surface of the sphere the fluid velocity matches the local velocity of the solid surface (since the spheres do not rotate this is the linear particle velocity $\boldsymbol{v}_p$); in the forcing scheme this is accomplished by imposing additional forces on the fluid at the surface of the solid sphere (which is then distributed to the lattice nodes in the vicinity of the particle surface). The details of the implementation can be found elsewhere.[16,17]

In our simulations, the diameter of each spherical particle is specified and input diameter refers to this diameter scaled by the lattice spacing. In the LB simulations, as the spherical particle is represented by forces that are confined to a cubic grid, the input diameter does not reflect the actual diameter of the particle. A calibration procedure to estimate the effective diameter of this object (commonly referred to as the hydrodynamic diameter) was introduced by Ladd.[19] We apply this scheme to estimate the hydrodynamic diameter of the particles. The hydrodynamic diameter is recognized as the diameter d_p mentioned earlier.

The dispersion of the passive scalar dissolved in the continuous phase fluid is simulated by numerically solving a convection-diffusion equation for the scalar concentration c. For this an explicit finite volume representation on the same grid as used by the LBM is employed. To limit numerical diffusion, we apply TVD discretization with the Superbee flux limiter for the convective fluxes.[20] We step in time according to an (second order) Adams-Bashford scheme. The molecular diffusion has been set to zero. We do not allow scalar concentration inside the spherical particles. At the surface of the particles, we impose the $\frac{\partial c}{\partial n} = 0$ condition by means of a ghost-cell technique[21] that involves interpolation of scalar concentrations.

The condition $\frac{\partial c}{\partial n} = 0$ is also applied for assigning concentrations to grid nodes that get uncovered by a moving solid particle. Since particles typically move less than 0.05 times the lattice spacing per time step, an uncovered node always is close to a solid particle interface. We draw the normal out of the particle into the fluid at the position of the uncovered node. By interpolation we determine the concentration on the normal one additional grid spacing into the fluid and assign that concentration to the uncovered node. In some situations this cannot be done: it regularly occurs that a grid cell gets uncovered in between two closely spaced particles moving away from each other after a collision. The outward normal from one particle then quickly penetrates the other particle where no concentration data is available. In such cases we assign the average concentration in the direct vicinity to the uncovered grid node, while keeping that vicinity as small as possible. Particles covering and uncovering grid nodes

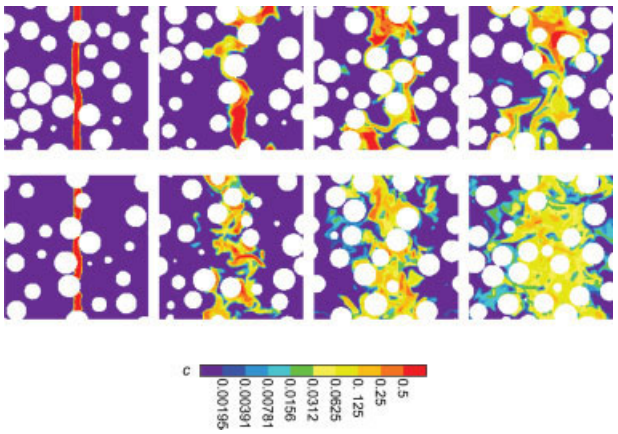

Figure 1. Snapshots of concentration contours in *xz* cross sections through the cubic domain.

The white disks represent the particles that all have the same size but different distance to the plane of cross section. Top four panels: $\phi = 0.30$ and $Re_g = 2.8$ at (from left to right) $\frac{t\sqrt{(T_g)}}{d_p} = 0.05$, 1.96, 3.88, and 5.79 respectively. Bottom four panels have the same parameters except now $Re_g = 104$. [Color figure can be viewed in the online issue, which is available at www.interscience.wiley.com.]

containing concentration information makes the simulations not inherently mass conservative. In practice, however, the total scalar mass over a simulation is constant within 0.2%.

We consider passive scalar transport in a fully developed flow of particles and fluid. As initial condition for the scalar concentration we give a thin *yz*-slab (with slab thickness $d_p/4$) of fluid a concentration $c = 1$, and the rest of the fluid $c = 0$. Subsequently we keep track of the spreading of the scalar as a result of the fluid flow induced by the solid particle motion. Typical sequences are given in Figure 1. The full, three-dimensional data is reduced to a one-dimensional scalar concentration function $\tilde{c}(x,t) \equiv \frac{1}{L^2}\int_0^L\int_0^L c(x,y,z,t)dydz$. By repeating the simulation M times and averaging the results we get smooth $\tilde{c}(x,t)$ profiles that we fit with a Gaussian $\tilde{c}_{\text{fit}}(x,t) = \frac{a}{\sigma(t)\sqrt{2\pi}}\exp\left(\frac{(x-\mu)^2}{2\sigma(t)^2}\right)$, see Figure 2. The default value of the number of repetitions M has been set to 20. The only fitting parameter is σ; the other two parameters (a and μ) are a priori known and constant in time. They relate to the total scalar mass released (a), and the average position of the scalar μ (which is the center position of the initial slab). We use the way σ develops in time as a measure for the scalar dispersion.

In Figure 2 we see that for "short" times the simulated concentration profile does not fit a Gaussian very well. This is due to the top-hat initial concentration profile we imposed. At later stages, however, the profiles are very much akin to Gaussian functions, and the width of the fitted Gaussian is a good measure for the scalar spreading.

Numerical Settings

The solids volume fractions that have been considered are $\phi = 0.10$, 0.20, 0.30, 0.373, and 0.45. The cases with $\phi = 0.30$ served as base cases. Verification tests regarding reproducibility, grid refinement, time step, and domain size were performed at this volume fraction. For each volume fraction we vary the Reynolds number based on the granular temperature (Re_g) by varying the fluid viscosity. The Reynolds numbers considered are 2.8, 28, 104, and 280.

The default values for the particle diameter d_p is 16 lattice spacings ($d_p = 16$ in LB units). The default domain size $L = 100$ ($L = 6.25\ d_p$). The number of spheres in the computational domain determines ϕ. The granular temperature is chosen such that the solid particle velocities (a good measure of which is $\sqrt{T_g}$) stay well below the speed of sound of the lattice-Boltzmann scheme: T_g is of the order of 10^{-4}, the speed of sound is of order 1.

Results

Verifications

A number of verification tests were performed for cases with $\phi = 0.30$. In the first place we checked reproducibility, i.e. if the size of the ensemble M (=20) that we base our fitting procedure on is large enough to get reproducible results. In conjunction with reproducibility we checked the influence of the domain length in x-direction. As can be seen in Figures 1 and 2, at some stage in time the concentration profile gets a width comparable to the size L of the domain. The periodic conditions then make the scalar leaving the domain on the right hand side enter on the left hand side, inhibiting a fit with a single Gaussian. One of the options for extending the time span of some of the simulations is enlarging the domain size in x-direction. Figure 3 shows results on reproducibility and on the effect of doubling the domain size in x-direction in the form of evolutions of σ as a function of time. The σ vs. t curves are well reproducible (deviations less then 4%). Extending the domain size allows for longer

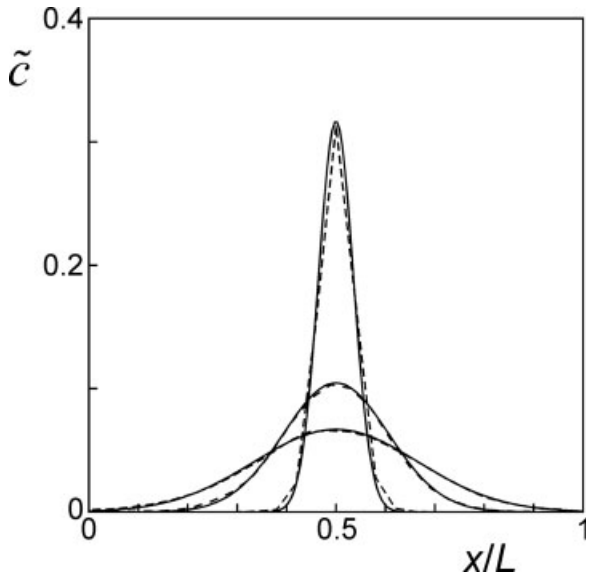

Figure 2. Simulated (dashed lines) and fitted (solid lines) one-dimensional concentration profiles at three instants in time.

$\frac{t\sqrt{(T_g)}}{d_p} = 0.43$, 2.16, and 4.33. $\phi = 0.30$ and $Re_g = 104$.

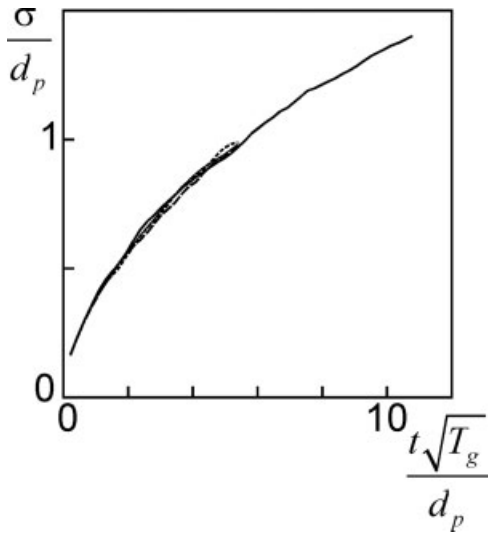

Figure 3. Concentration profile width σ as a function of time for three statistically independent repetitions with $\phi = 0.30$ and $Re_g = 2.8$ on a cubic L^3 domain (thin solid curve, dotted curve, dashed curve).

The thick solid curve has the same settings except for the domain size in x-direction and the time span of the simulations. Both were doubled.

runs thus getting a clearer view on the functional relationship between the concentration profile width and time.

With a view to (numerical) diffusion the effect of spatial resolution should be checked. In the simulations, the molecular diffusion has been set to zero in order to only probe the effect of the particle motion and associated fluid flow on spreading the scalar. Inevitably however, numerical diffusion takes place, and will potentially broaden the concentration profiles in an unphysical manner. Since numerical diffusion is a pronounced function of the grid spacing, systematically refining the grid gives us insight in to what extent the results of the simulations are affected by numerical diffusion. We carried out simulations at $\phi = 0.30$ at three levels of resolution: $d_p = 12$, 16, and 24, and show results in Figure 4. The mutual differences between the curves are slightly higher than the levels of statistical uncertainty (the latter to be estimated from Figure 3). Also the curve with the highest resolution ($d_p = 24$) is systematically below the curves related to coarser grids, indicating some numerical diffusion effects (although this may be counteracted by the fact that the $d_p = 16$ curve is mostly above the $d_p = 12$ curve). We conclude that if there is an effect of numerical diffusion on the scalar spreading rate, its extent is a few percent at most.

The next check relates to the temporal resolution of the simulations. In terms of numerical (LB) units, the time step actually is the time unit: $\Delta t = 1$. The physical conditions are fully defined by the solids volume fraction and the granular Reynolds number. At a specific spatial resolution this leaves us one degree of freedom which is the time step related to physical terms. We can choose the granular temperature (and then the viscosity is fixed through the required Reynolds number), or vice versa. The higher the granular temperature (and thus the higher the viscosity), the greater the time step

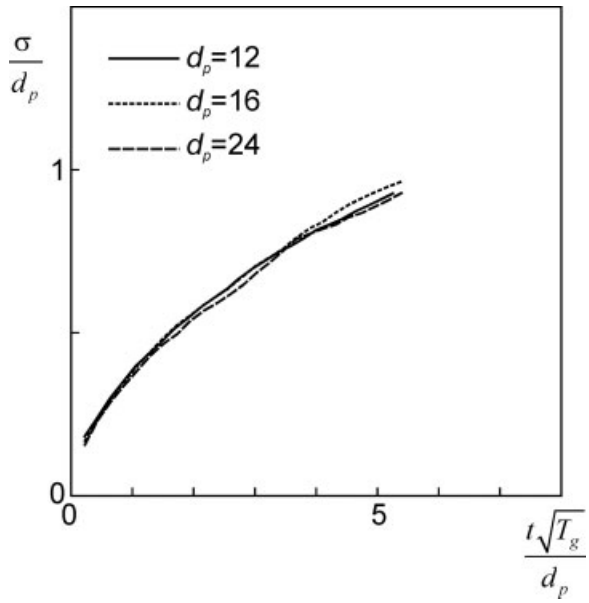

Figure 4. Concentration profile width σ as a function of time at three levels of spatial resolution for $\phi = 0.30$ and $Re_g = 2.8$.

in physical terms. In the two simulations of which the spreading results are shown in Figure 5, the solids volume fraction ($\phi = 0.30$), the Reynolds number ($Re_g = 2.8$) and the spatial resolution ($d_p = 16$) are the same. In one case the Reynolds number was reached by setting $T_g = 2.98 \times 10^{-4}$ and $v = 0.1$, in the other by $T_g = 7.45 \times 10^{-5}$ and $v = 0.05$. In the latter case the time step in physical terms is twice as

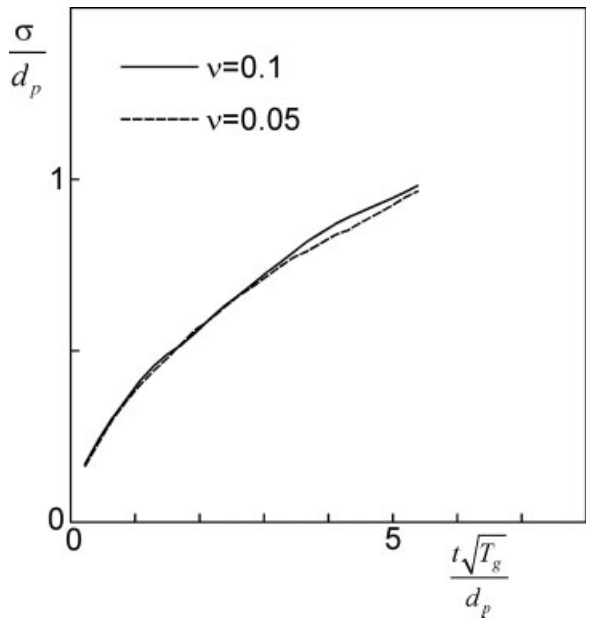

Figure 5. Concentration profile width σ as a function of time for $\phi = 0.30$ and $Re_g = 2.8$.

The curve denoted by $v = 0.1$ has a twice as large time step in physical terms as the curve with $v = 0.05$ (see the text for details).

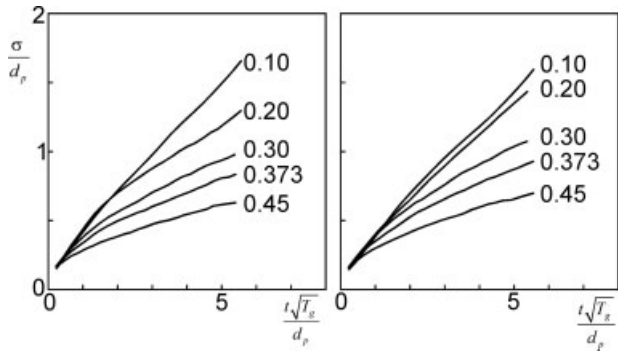

Figure 6. Concentration profile width σ as a function of time for various solids volume fractions.

Left panel: $Re_g = 2.8$; right panel: $Re_g = 28$.

small as in the former case. The difference between the two results is not significant in view of the statistical uncertainties that were discussed in relation to Figure 3.

Scaling scalar spreading

There is a very distinct effect of the solids volume fraction on scalar spreading. In Figure 6 we show that the scalar spreading increases significantly with decreasing solids volume fraction. This is not a surprising result. The mean-free-path (MFP, symbol λ) of the solid particles increases with decreasing solids volume fraction (for dilute gases this is an inversely proportional relationship). If the particles are able to travel longer in a certain direction, they take with them the scalar over longer distances. This notion suggests that it

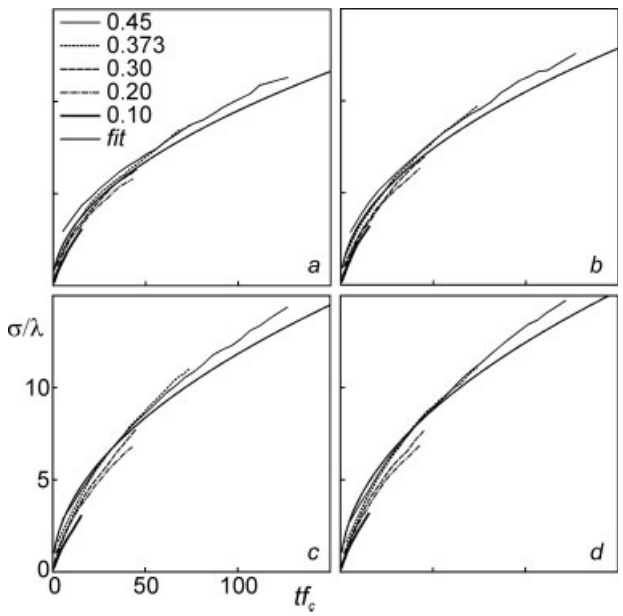

Figure 7. Concentration profile width σ as a function of time for various solids volume fractions.

Time has been scaled with the collision frequency f_c, σ with the MFP λ. Panels *a*, *b*, *c*, and *d* respectively have $Re_g = 2.8$, 28, 104, and 280. The fit also included is the function $\frac{\sigma}{\lambda} = \sqrt{\alpha t f_c}$. The fitting parameter α differs per panel and is 0.9, 1.1, 1.4, and 1.5, respectively.

Table 1. Characterization of the Granular Systems

ϕ (−)	T_g (LB units)	λ (LB units)	f_c (LB units)
0.10	$3.18 \cdot 10^{-4}$	14.9	$1.56 \cdot 10^{-3}$
0.20	$3.18 \cdot 10^{-4}$	5.40	$4.31 \cdot 10^{-3}$
0.30	$2.98 \cdot 10^{-4}$	2.49	$9.05 \cdot 10^{-3}$
0.373	$3.01 \cdot 10^{-4}$	1.53	$1.48 \cdot 10^{-2}$
0.45	$3.01 \cdot 10^{-4}$	0.891	$2.54 \cdot 10^{-2}$

All systems in this table have cubic periodic domains with $L = 100$ (LB units), and uniformly sized particles with $d_p = 16$ (LB units).

makes sense to scale the scalar spreading as a function of time in terms of collisional parameters, viz. the MFP and the collision frequency of the particles. This we do in Figure 7. It shows the scalar spreading as a function of time for all the four Reynolds numbers we have considered. The MFP λ and the collision frequency f_c were directly determined from the simulations. Their values are given in Table 1. For each Reynolds number, the curves taken at different solids volume fraction get quite close to one another. There is a systematic difference though. The curves related to the higher solids volume fractions are slightly but systematically above the ones with lower ϕ; apparently the scaling with λ and f_c slightly overcompensates the differences as observed when scaling with d_p and $\frac{d_p}{\sqrt{T_g}}$ (Figure 6). Note that for increasing the dimensionless time span $t \cdot f_c$ of the simulations with the lower solids volume fractions we made use of simulations on domains that where twice as long in the x-direction (compared to the two lateral (y and z) directions), as well as in LB time.

Also shown in Figure 7 is the (by the eye) best fit through the bundle of curves according to the function $\frac{\sigma}{\lambda} = \sqrt{\alpha t f_c}$, with α the only fitting parameter. We estimate this rather coarse way of fitting to be roughly $\pm 8\%$ accurate in α. We see that despite the uncertainties involved, the dimensionless parameter α clearly depends on the granular Reynolds number. Figure 8 shows a plot of α versus $^{10}\log(Re_g)$. Based on the trend lines in this graph we speculate that for low Reynolds numbers ($Re_g \leq 10$) α is constant, and that for higher

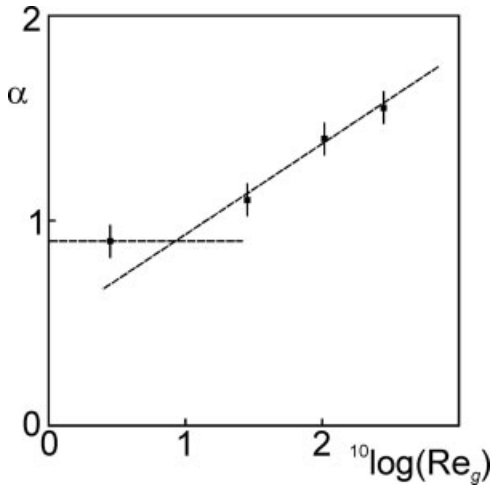

Figure 8. Fit parameter α as a function of the granular Reynolds number Re_g.

The dashed lines indicate trends.

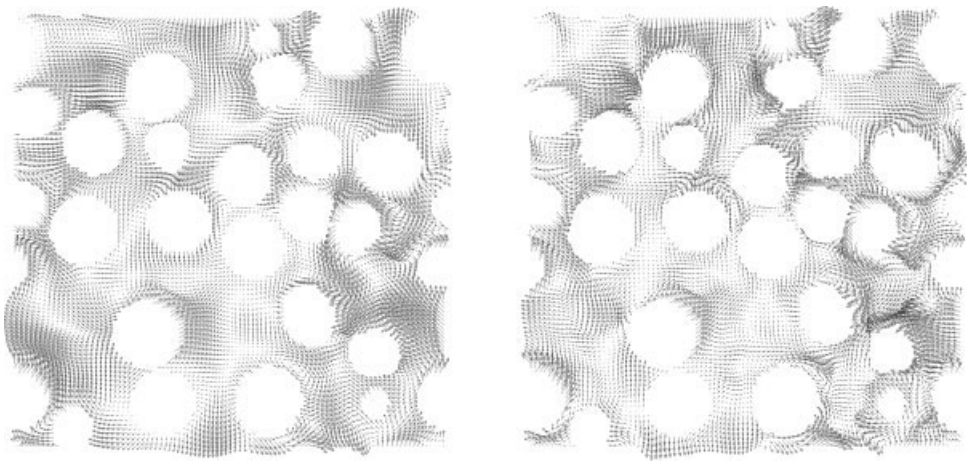

Figure 9. Cross sections through the flow domains in terms of fluid velocity vectors for $\phi = 0.373$.

Left, $Re_g = 2.8$; right, $Re_g = 104$. Both panels have exactly the same particle configuration (particle positions and velocities), and the same fluid velocity vector scaling.

Re_g α could be linearly increasing with $^{10}\log(\mathrm{Re}_g)$. In Figure 9 we show snapshots of the fluid velocity vector field in a cross section through the flow domains at two different Reynolds numbers. The two panels are at exactly the same particle configuration (particle positions and velocities). For low Reynolds numbers the fluid flow and thus the scalar spreading are largely slaved to the kinematics of the particle motion; the flow does not develop structures smaller than those related to the particle field (see Figure 9a). At higher Reynolds numbers, the now more inertial flow develops eddies that play a role in enhancing scalar spreading, see Figure 9b.

If the scalar spreading were a process that could be described with a single effective diffusion coefficient D, the way σ depends on time is $\sigma = \sqrt{2Dt}$. Relating that to the way we fitted our scalar spreading results ($\frac{\sigma}{\lambda} = \sqrt{\alpha t f_c}$) gives $D = \frac{1}{2}\alpha\lambda^2 f_c$. The latter expression along with a functional relationship for the dependence of α on Re_g could serve as closure for the dispersion term in the scalar transport equation to be solved in conjunction with e.g. DPM simulations, or Euler-Euler simulations of gas–solid or liquid–solid flows.

A from a theoretical viewpoint interesting situation occurs in the limit $\phi \to 0$. Since $\lambda \propto \phi^{-1}$, and $f_c \propto \phi$, in this limit the effective diffusion coefficient $D = \frac{1}{2}\alpha\lambda^2 f_c$ would go to infinity. This divergence is due to the concept of diffusion that requires particles to collide with one another (or with bounding walls). If particles do not collide, the scalar is essentially convected by the moving particles and σ tends to get proportional to time (instead of proportional to $\sqrt{t}$).

Summary

In this article we discussed mixing as a result of solid particle motion. We set up fully resolved, one-way coupled numerical simulations: moving spherical particles immersed in a fluid drive fluid motion; the interstitial fluid, however, does not influence the particle motion. This way we could control the conditions of the numerical experiment and could focus on the impact of two key variables (viz. the solids volume fraction, and the granular Reynolds number) on scalar spreading. To limit the parameter space, the role of molecular diffusion of the passive scalar was not considered in this paper. The scalar was supposed to have zero molecular diffusivity (infinite Schmidt number limit).

First the numerical procedure was verified. A grid refinement study revealed largely grid independent results, which demonstrated that spreading is hardly due to numerical diffusion. Furthermore, the scalar spreading was shown to be reproducible, and independent of other numerical settings.

The results show that scalar spreading increases with decreasing solids volume fraction, and increases with increasing granular Reynolds number. The former effect is thought to be due to the longer mean-free-path (MFP) λ for lower solids volume fractions. The longer the MFP, the more effectively the scalar is carried around. Indeed, if we scale the scalar spreading as a function of time with particle collision parameters (the collision frequency, and the MFP), the spreading functions become more universal. However, there clearly is no complete universality. Especially the lower solids volume fraction (≤ 0.2) cases deviate from the "master curve."

A tentative fit of the scalar spreading with a $\sqrt{t}$-function showed that the effective diffusion coefficient could be written as $D = \frac{1}{2}\alpha\lambda^2 f_c$, with f_c the collision frequency, and α a parameter of the order 1 which depends on the granular Reynolds number. In the range of Reynolds numbers considered in this paper, α is a monotonically rising function of Re_g. The increase of α is due to the development of small-scale flow structures at higher Reynolds numbers.

Future research will focus on the role of particle rotation in scalar spreading, and on the effects a particle size distribution (as opposed to monosized particles) might have. Furthermore, we will apply the engineering correlations for scalar dispersion that were proposed here to scalar spreading in inhomogeneous systems such us fluidized beds. For the meso-scale we could compare (scalar transport in) direct simulations of liquid-solid fluidization,[22] with ones employing closure relations.

Literature Cited

1. Gidaspow D. *Multiphase Flow and Fluidization*. San Diego CA: Academic Press, 1994.
2. Jackson R. *Dynamics of Fluidized Particles*. Cambridge: Cambridge University Press, 2000.
3. Hoomans BPB, Kuipers JAM, Briels WJ, Van Swaaij WPM. Discrete particle simulation of bubble and slug formation in a two-dimensional gas-fluidized bed: a hard-sphere approach. *Chem Eng Sci*. 1996;51:99–118.
4. Dahl SR, Hrenya CM. Size segregation in gas-solid fluidized beds with continuous size distributions. *Chem Eng Sci*. 2005;60:6658–6673.
5. Moon SJ, Sundaresan S, Kevrekidis IG. Coarse grained computations of demixing in dense gas-fluidized beds. *Phys Rev E*. 2007; 75:051309.
6. Levenspiel O. *Chemical Reaction Engineering*, 2nd ed. New York: Wiley, 1962.
7. Sotudeh-Gharebaagh R, Chaouki J. Gas mixing in a turbulent fluidized bed reactor. *Can J Chem Eng*. 2000:78;65–74.
8. Al-Sherehy F, Grace J, Adris A-E. Gas mixing and modeling of secondary gas distribution in a bench-scale fluidized bed. *AIChE J*. 2004:50;922–936.
9. Deshmukh SARK, Van Sint Annaland M, Kuipers JAM. Gas backmixing studies in membrane assisted bubbling fluidized beds. *Chem Eng Sci*. 2007:62;4095–4111.
10. Harten A. High resolution schemes for hyperbolic conservation laws. *J Comp Phys*. 1983:49;357–364.
11. Chen S, Doolen GD. Lattice Boltzmann method for fluid flows. *Ann Rev Fluid Mech*. 1998:30;329–364.
12. Succi S. *The Lattice Boltzmann Equation for Fluid Dynamics and Beyond*. Oxford: Clarondon Press, 2001.
13. Somers JA. Direct simulation of fluid flow with cellular automata and the lattice-Boltzmann equation. *Appl Sci Res*. 1993:51;127–133.
14. Qian YH, d'Humieres D, Lallemand, P. Lattice BGK for the Navier-Stokes equations. *Europhys Lett*. 1992:17;479–484.
15. Goldstein D, Handler R, Sirovich L. Modeling a no-slip flow boundary with an external force field. *J Comp Phys*. 1993:105;354–366.
16. Derksen JJ, Van den Akker HEA. Large eddy simulations on the flow driven by a Rushton turbine. *AIChE J*. 1999:45;209–221.
17. Ten Cate A, Nieuwstad CH, Derksen JJ, Van den Akker HEA. PIV experiments and lattice-Boltzmann simulations on a single sphere settling under gravity. *Phys Fluids*. 2002:14;4012–4025.
18. Griffith BE, Peskin CS. On the order of accuracy of the immersed boundary method: higher order convergence rates for sufficiently smooth problems. *J Comp Phys*. 2005:208;75–105.
19. Ladd AJC. Numerical simulations of particle suspensions via a discretized Boltzmann equation. I. Theoretical Foundation. *J Fluid Mech*. 1994:271;285–309.
20. Sweby PK. High resolution schemes using flux limiters for hyperbolic conservation laws. *SIAM J Numer Anal*. 1984;21:995–1011.
21. Hartmann H, Derksen JJ, Van den Akker HEA. Mixing times in a turbulent stirred tank by means of LES. *AIChE J*. 2006:52;3696–3706.
22. Derksen JJ, Sundaresan S. Direct numerical simulations of dense suspensions: wave instabilities in liquid-fluidized beds. *J Fluid Mech*. 2007:587;303–336.

Manuscript received Sept. 13, 2007, and revision received Apr. 13, 2008.